

Ionization fronts and their interaction with density fluctuations: implications for reionization

Ilian T. Iliev¹, Paul R. Shapiro², Evan Scannapieco³, Garrelt Mellema⁴, Marcelo Alvarez², Alejandro C. Raga⁵, and Ue-Li Pen¹

¹ Canadian Institute for Theoretical Astrophysics, University of Toronto, 60 St. George Street, Toronto, ON M5S 3H8, Canada, email: iliev@cita.utoronto.ca

² Department of Astronomy, University of Texas, Austin, 78712, USA

³ Kavli Institute for Theoretical Physics, Kohn Hall, UC Santa Barbara, Santa Barbara, CA 93106, USA

⁴ ASTRON, P.O. Box 1, NL-7990 AA Dwingeloo, The Netherlands

⁵ Instituto de Ciencias Nucleares, Universidad Nacional Autónoma de México (UNAM), Apdo. Postal 70-543, 04510 México, D. F., México

Abstract.

The propagation of cosmological ionization fronts (I-fronts) during reionization is strongly influenced by small-scale structure. Here we summarize our recent attempts to understand the effect of this small-scale structure. We present high resolution cosmological N-body simulations at high- z ($z > 6$) which resolve a wide range of halo mass, from minihalos to clusters of large, rare halos. We also study how minihalos affect I-fronts, through simulations of minihalo photoevaporation by numerical gasdynamics with radiative transfer. Furthermore, we modify the I-front propagation equations to account for evolving small-scale structure, and incorporate these results into a semi-analytical reionization model. When intergalactic medium clumping and minihalo clustering around sources are included, small-scale structure affects reionization by slowing it down and extending it in time. This helps to explain observations by the Wilkinson Microwave Anisotropy Probe, which imply an early and extended reionization epoch. We also study how source clustering affects the evolution and size of H II regions, finding, in agreement with simulations, that H II regions usually expand, rarely shrinking. Hence, “relic H II regions” are an exception, rather than the rule. When the suppression of small-mass sources in already-ionized regions by Jeans-mass filtering is accounted for, H II regions are smaller, delaying overlap. We also present a new numerical method for radiative transfer which is fast, efficient, and easily coupled to hydrodynamics and N-body codes, along with sample tests and applications.

Keywords. hydrodynamics, radiative transfer, HII regions, intergalactic medium, galaxies: formation, galaxies: high-redshift, galaxies: statistics, cosmic microwave background, cosmology: theory

1. Introduction

When a source of ionizing radiation turns on in a neutral gas, the I-front initially moves supersonically as a weak, R-type front and outruns the gas dynamical disturbance it creates (e.g. Spitzer 1978, and refs. therein). In a uniform gas, the front eventually slows to twice the isothermal sound speed of the ionized gas as it approaches the size of the equilibrium Strömgen sphere and is transformed into a subsonic D-type front, usually preceded by a shock. Thereafter, it is very much affected by gas dynamics. Shapiro & Giroux (1987) first considered this problem in the cosmological context of the expanding IGM, deriving

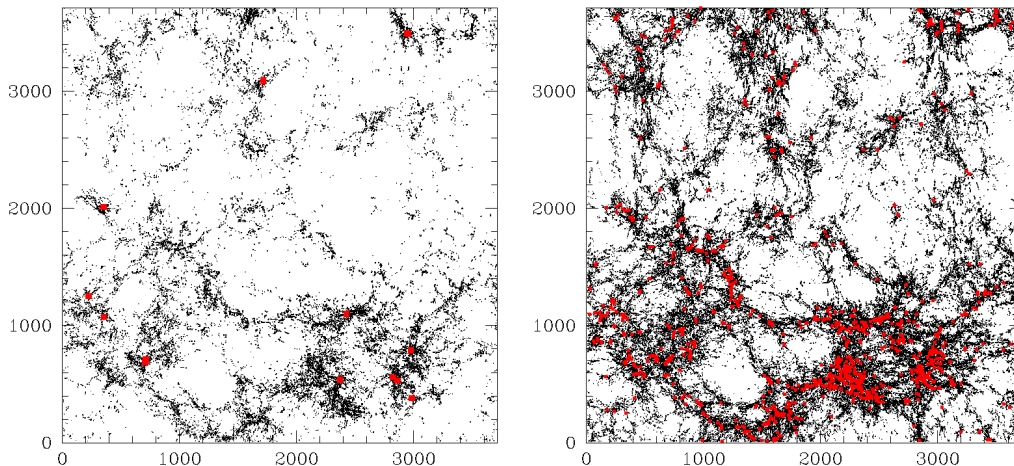


Figure 1. Structure formation at high redshift in Λ CDM. Halo distribution at (left) redshift $z = 17.2$ and (right) $z = 9.42$ from massively-parallel PMFAST N-body simulation with 1836^3 particles, 3672^3 cells, simulation box size $10h^{-1}$ Mpc comoving. Shown are minihalos (black dots) and ionizing sources (red squares) in a 1 Mpc thick slice (approx. 1/14th of the total simulation volume).

the general equations describing I-front evolution and solving them analytically for the case of constant gas clumping factor and temperature. They found that global cosmological I-fronts typically stayed in the weak, R-type regime as the density dropped over time, failing to reach the Strömgen radius. This result justifies subsequent approximate treatments of cosmic reionization in the inhomogeneous IGM that results from structure formation which neglect the gasdynamical back reaction of the I-fronts. However, when the I-fronts encounter self-shielding inhomogeneities (like halos) large and dense enough to trap the I-fronts and convert them to D-type, this approximation must break down.

2. Structure formation at high redshift and its effects on I-front propagation during reionization

Within the CDM paradigm cosmological structures form hierarchically in time, starting with the smallest-scale structures at the highest redshifts, which grow through accretion and mergers to form larger and larger structures. While the cold dark matter clumps gravitationally on all scales, only virialized halos with total mass above the cosmological Jeans mass can retain their gas content. These virialized halos can be divided into two main classes, halos with virial temperature above $\sim 10^4$ K whose gas can cool through atomic line cooling of hydrogen, leading to efficient star formation in such halos, and smaller-mass halos (minihalos) whose gas in absence of metals can only cool through H_2 molecules, which are fragile and easily destroyed. Thus, the first class of halos are generally believed to be the dominant sources of the radiation responsible for cosmic reionization, while typical minihalos were unable to form stars once the first generation created a background of dissociating UV starlight. Subsequently, minihalos were just inert balls of neutral gas. Figure 1 shows the halos which formed in a large N-body simulation of early structure formation. The larger (source) halos (red squares) are quite rare and highly clustered, especially at high redshift, as expected for rare density peaks in a Gaussian density field. On the other hand, the minihalos (black dots) are quite common

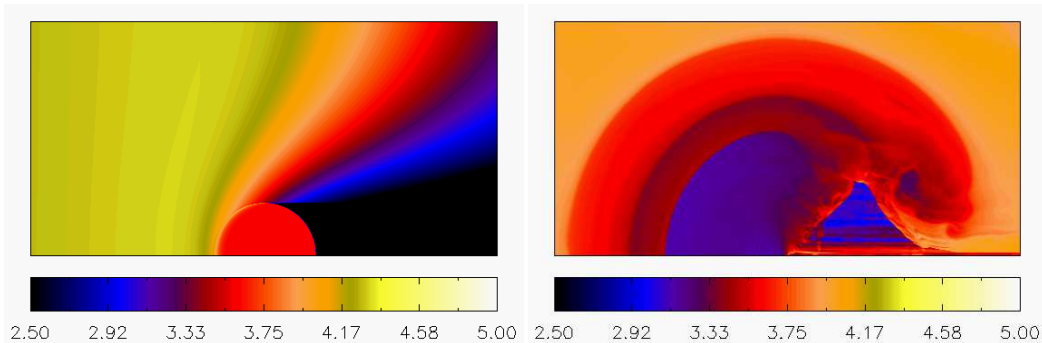


Figure 2. Photoevaporating minihalo snapshots of temperature for $10^7 M_{\odot}$ minihalo encountered by a global I-front at $z = 9$ from a source with 50,000 K black-body spectrum. Times shown are: (left) 0.2 Myr, when I-front is still fast, R-type, with extended structure in IGM due to the finite photon mean free path clearly visible, and (right) 150 Myr, close to the complete evaporation, after which only a dark halo devoid of gas remains. Note complex flow structure which involves multiple shocks. Shaded isocontours indicate the values of $\log_{10}(T)$, as labeled on the color bar.

at all times and are strongly clustered around the ionizing sources, covering their sky (Shapiro 2001).

I-fronts propagating outward from the ionizing sources encounter these minihalos and get trapped inside them, eventually completely photoevaporating all the gas. We have studied this process in detail, by means of high-resolution adaptive-mesh-refinement (AMR) hydrodynamic and radiative transfer simulations (Shapiro et al. 2004; Iliev et al. 2005d). In Figure 2 we show two snapshots of the photoevaporative flow’s temperature structure at times $t = 0.2$ Myr (during the fast, R-type phase), showing the relatively extended I-front structure compared to the minihalo size, and $t = 150$ Myr, close to the moment of complete evaporation of the minihalo, which shows the complicated structure of the photoevaporative flow, with multiple shocks (see papers for details). We have performed a large number of these high-resolution simulations (with finest grid up to $(r, z) = 1024 \times 2048$ in 2-D axisymmetry) and found simple analytical fits to the total consumption of ionizing photons and evaporation times as functions of the minihalo initial mass, redshift, and the flux and spectrum of the ionizing source (Iliev et al. 2005d). We showed that minihalos can increase the global ionizing photon consumption during reionization by a factor of up to 2 compared to the mean IGM alone.

Using our fitting formulae to our detailed simulation results, we were able to modify the I-front propagation equations of Shapiro & Giroux (1987) to properly reflect the increased consumption of ionizing photons due to the minihalos and the corresponding slowing down of the global I-fronts (Iliev et al. 2005c). We included the effects of infall and minihalo bias around the sources, the evolving mean IGM clumping and the dependence on the photon production efficiencies, spectra and lifetimes of the ionizing sources. We found that small-scale structures have a significant effect on the progress of reionization, slowing it down and extending it in time, which can help us understand the recent observations by the Wilkinson Microwave Anisotropy Probe satellite, which point to an early and extended reionization epoch (Fig. 3). More recently (work in progress) we extended our formalism to account for the clustering of the ionizing sources. We find that the clustering of source halos in time and space leads to multiple sources in each H II region, which dramatically changes the numbers and sizes of the ionized regions and hence the overall topology of reionization (Fig. 4 and Fig. 5, left). H II regions around short-lived individual sources are small (less than 1 Mpc comoving around the smaller sources) and quickly recombine and shrink in size once the source ends its life, forming so-

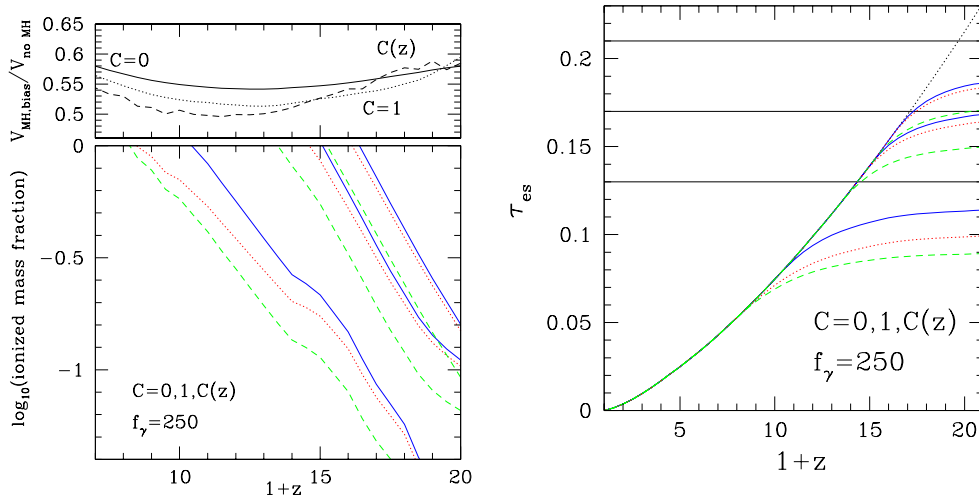


Figure 3. Global reionization. Sources with $f_{\gamma} = 250$ and lifetime of $t_s = 3$ Myr are assumed. (bottom panel) Decimal logarithm of ionized mass (or Lagrangian volume) fractions (i.e. 0 corresponds to overlap) for the cases of no minihalos (solid), unbiased minihalos (dotted), and biased minihalos (dashed) for IGM clumping factors (top to bottom in each case) $C = 0, 1$, and $C(z)$ (clumped IGM). (upper panel) Ratios of the ionized volume fractions in the presence of *biased* minihalos and with no minihalos for $C = 0, 1, C(z)$

called “relic H II regions”, but when source halo clustering is taken into account the H II regions expand continuously, reaching sizes of up to tens and hundreds of comoving Mpc. In that case, relic H II regions do not generally form. We also study the consequences of the suppression of the formation of smaller sources inside the already-ionized regions (due to increased Jeans mass there, in correspondence to the higher gas temperature of $\sim \text{few} \times 10^4$ K) (Fig. 5, right). We find that sufficiently strong suppression can have quite dramatic effects, decreasing (in the particular high-redshift source case we consider here) the size of the H II region by an order of magnitude, and leading to a temporary formation of a small relic H II region. However, for lower-redshift sources this suppression has much smaller consequences since the larger ionizing sources (whose formation is not affected by this suppression), which were very rare at high- z , become more abundant and start playing a more important role in the process of reionization.

3. A new photon-conserving method for transfer of ionizing radiation

In the last few years there has been an intense development of new numerical radiative transfer methods for cosmology (e.g. Abel et al. 1999; Gnedin & Abel 2001; Razoumov et al. 2002; Maselli et al. 2003). However, most of the existing methods are not efficient enough to be directly coupled to gas- and N-body dynamics, which limits the scope of their applications. One common problem is that the fast, R-type I-front propagation timescale (sometimes approaching the light-crossing time) is much shorter than the fluid dynamical and gravitational times, leading to the necessity of very small time-steps to track the I-fronts correctly. In addition, the bound-free opacity of the neutral gas is very high, so algorithms for spatial differencing the transfer equation often require very small cell sizes, and this implies very small time steps even when the I-fronts are subsonic. Our photoevaporation simulations described above (Shapiro et al. 2004; Iliev et al. 2005d) utilized an AMR Eulerian hydro code in 2-D axisymmetry, capable of handling a large range of scales with high resolution efficiently enough that we were able to take very small time-

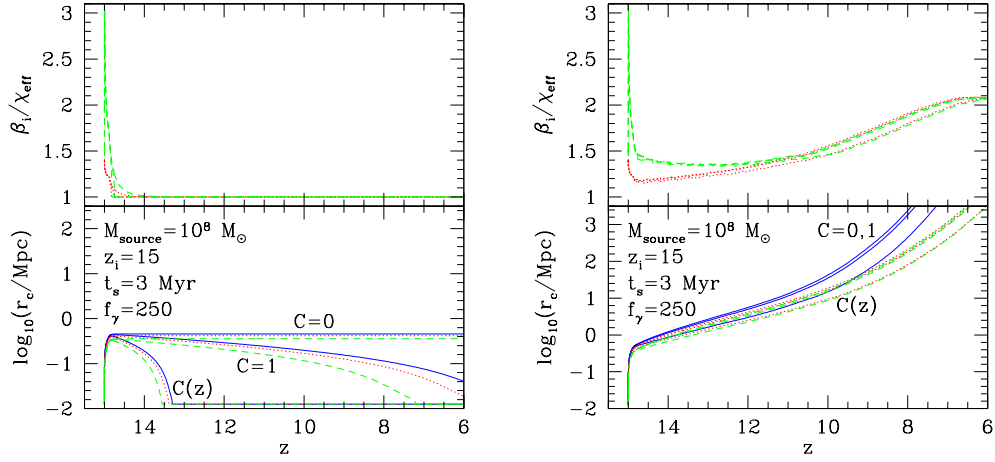


Figure 4. Evolution of an individual H II region about a central source of mass $10^8 M_\odot$ which turns on at redshift $z = 15$, for (left) a single source, and (right) clustered multiple sources for $C = 0, 1, C(z)$. *Top:* The correction factor $\beta_i/\chi_{\text{eff}}$ due to minihalos for the number of ionized photons consumed per atom that crosses the I-front, for biased (dashed) and unbiased minihalos (dotted). *Bottom:* Comoving radius of the H II region for no minihalos (solid), unbiased (dotted) and biased minihalos (dashed).

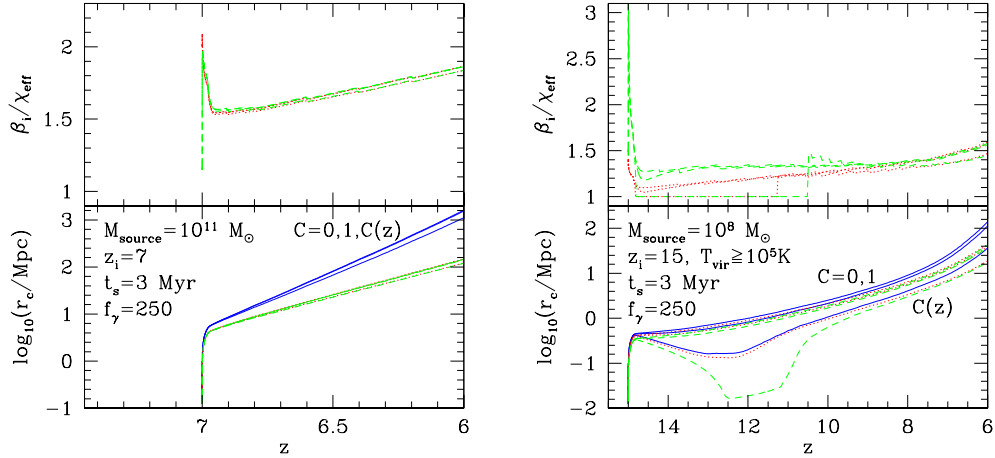


Figure 5. Same as Fig. 4, for clustered sources, but (left) a central source of mass $10^{11} M_\odot$ turning on at $z = 7$, and (right) assuming that the formation of ionizing sources with virial temperatures below 10^5K is suppressed within the H II region.

steps and very small cell sizes where needed. However, to generalize these “zoomed-in” calculations to 3-D and a simulation volume large enough to encompass both small- and large-scale structure, it is necessary to develop a more sophisticated radiative transfer algorithm. We have recently developed such a method, which accurately follows both fast and slow I-fronts without need to adopt such small time-steps or cell sizes. We achieved this by matching the ionization rates and flux attenuation along rays to ensure photon conservation, and time-averaging the neutral column densities per cell per step to give the correct I-front position and speed even for large time-steps and cell-widths (Mellema et al. 2005; Iliev et al. 2005b) (see papers for details). These characteristics

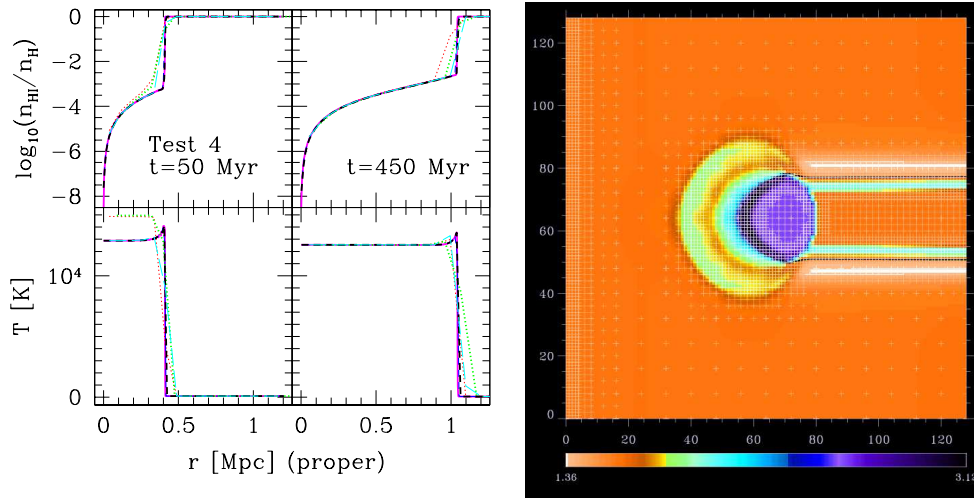


Figure 6. Photon-conserving RT. (left) Neutral hydrogen (top) and temperature (bottom) profiles for cosmological I-front starting at $z = 9$. The left panels show time $t = 50$ Myrs after turn-on ($= 1$ time step in coarse temporal resolution case, and 10 time steps in the high temporal resolution case), while right panels show solution at $t = 450$ Myrs ($= 3.5t_{\text{rec}}$). Thin lines correspond to 1-D results with 16 cells, 10 time-steps (dotted, red), 16 cells, 100 time-steps (long-dashed, cyan), and 128 cells, 100 time-steps (short-dashed, blue). Thick lines correspond to 3-D results with 32^3 cells, 10 time-steps (dotted, green) and 256^3 cells, 100 time-steps (short-dashed, black). Finally, the reference “exact” solution (1-D, 1024 cells, 100 time-steps) is shown by thick, solid, magenta line. (right) 3-D, AMR gasdynamics and radiative transfer simulation of photoevaporation of a dense gas clump calculated with a 5-level adaptive mesh. Snapshot shows $\log_{10}(n)$, gas number density in central xy plane. White crosses indicate computational mesh, while black shows I-front position.

make our method very efficient for direct coupling with gasdynamic and N-body codes. We have tested the method in detail, on both fixed and adaptive grids, as a stand-alone radiative transfer code as well as coupled to AMR gasdynamics (for some sample results see Fig. 6).

References

- Abel, T., Norman, M. L., & Madau, P. 1999, *ApJ*, 523, 66
 Gnedin, N. Y. & Abel, T. 2001, *New Astronomy*, 6, 437
 Iliev, I. T., Alvarez, M., Scannapieco, E., & Shapiro, P. R. 2005a, in preparation
 Iliev, I. T., Mellema, G., & Shapiro, P. R. 2005b, in preparation
 Iliev, I. T., Scannapieco, E., & Shapiro, P. R. 2005c, *ApJ*, in press, (astro-ph/0411035)
 Iliev, I. T., Shapiro, P. R., & Raga, A. C. 2005d, *MNRAS*, in press, (astro-ph/0408408)
 Maselli, A., Ferrara, A., & Ciardi, B. 2003, *MNRAS*, 345, 379
 Mellema, G., Iliev, I. T., Alvarez, M., & Shapiro, P. R. 2005, in preparation
 Razoumov, A. O., Norman, M. L., Abel, T., & Scott, D. 2002, *ApJ*, 572, 695
 Shapiro, P. R. 2001, in *AIP Conf. Proc.* 586: 20th Texas Symposium on relativistic astrophysics, p. 219
 Shapiro, P. R. & Giroux, M. L. 1987, *ApJ*, 321, L107
 Shapiro, P. R., Iliev, I. T., & Raga, A. C. 2004, *MNRAS*, 348, 753
 Spitzer, L. 1978, *Physical processes in the interstellar medium* (New York Wiley-Interscience, 1978)